AIAA/AAS Astrodynamics Specialist Conference and Exhibit
21 - 24 August 2006, Keystone, Colorado

AIAA 2006-6177

Solar Sail Trajectory Optimization for the Solar Polar Imager (SPI) Mission

Bernd Dachwald*
German Aerospace Center (DLR), 82234 Wessling, Germany

Andreas Ohndorf†
German Aerospace Center (DLR), 51170 Cologne, Germany

Bong Wie‡
Arizona State University, Tempe, AZ 85287, USA

The Solar Polar Imager (SPI) mission is one of several Sun-Earth Connection solar sail roadmap missions currently envisioned by NASA. A current SPI reference mission design is based on a 160 m × 160 m, 150 kg square solar sail assembly with a 250 kg spacecraft bus and a scientific payload of 50 kg (450 kg total mass), having a characteristic acceleration of 0.35 mm/s^2. Using a conservative solar sail film temperature limit of 100°C to constrain the solar distance ("cold" mission scenario), our transfer trajectory to the SPI target orbit (circular orbit at 0.48 AU solar distance with 75 deg inclination) approaches the sun closer (to about 0.4 AU solar distance) than a current reference trajectory and therefore, exploiting the larger solar radiation pressure, takes – even with a lower hyperbolic excess energy for interplanetary insertion – only 6.4 instead of 6.7 years. For a higher sail temperature limit of 240°C ("hot" mission scenario), the optimal transfer trajectory approaches the sun much closer (to about 0.22 AU solar distance), resulting in an even shorter transfer duration of only 4.7 years. Based on this "hot" mission scenario, we perform several mission tradeoffs to gain a deeper insight into the trade space of the SPI mission: different sail temperature limits, different characteristic accelerations, different interplanetary insertion energies, and different sail degradation behaviors are investigated.

I. Introduction

The Solar Polar Imager (SPI) mission is one of several Sun-Earth Connection solar sail roadmap missions currently envisioned by NASA. A similar solar sail mission, called Solar Polar Orbiter (SPO), is studied by ESA (Ref. 1). The objective of the SPI mission is to investigate the global structure and dynamics of the solar corona and to reveal the secrets of the solar cycle and the origins of solar activity (Refs. 2 and 3).

A current SPI reference mission design in Refs. 4 and 5 is based on a 160 m × 160 m, 150 kg square solar sail assembly with a 250 kg spacecraft bus and a scientific payload of 50 kg (450 kg total mass). The characteristic thrust (max. thrust at 1 AU) of the sailcraft is $F_c = 160$ mN, which yields a characteristic acceleration (max. acceleration at 1 AU) of $a_c = 0.35\,\mathrm{mm/s^2}$. The SPI target orbit is a heliocentric circular orbit at 0.48 AU (in 3:1 resonance with Earth) with an inclination of 75 deg (although different target inclinations have been considered in various previous SPI mission studies). The current reference trajectory from Refs. 4 and 5 is shown in Fig. 1. After being placed onto an Earth-escape trajectory (with a hyperbolic excess energy of $C_3 = 0.25\,\mathrm{km^2/s^2}$) by a conventional launch vehicle such as a Delta II, the solar sail is to be deployed. It was first found by Wright in Refs. 6 and 7 and further examined by Sauer in Ref. 8 that the best way to perform a large inclination change with a solar sail is to first spiral inwards to a close solar distance, and

*Scientist, German Space Operations Center, Mission Operations Section, Oberpfaffenhofen, bernd.dachwald@dlr.de, +49-8153-28 2772, Member AIAA, Member AAS.
†PhD Student, Institute of Space Simulation, Cologne, andreas.ohndorf@dlr.de, +49-2203-601 2877.
‡Professor, Dept. of Mechanical & Aerospace Engineering, bong.wie@asu.edu, +1-480-965 8674, Associate Fellow AIAA.

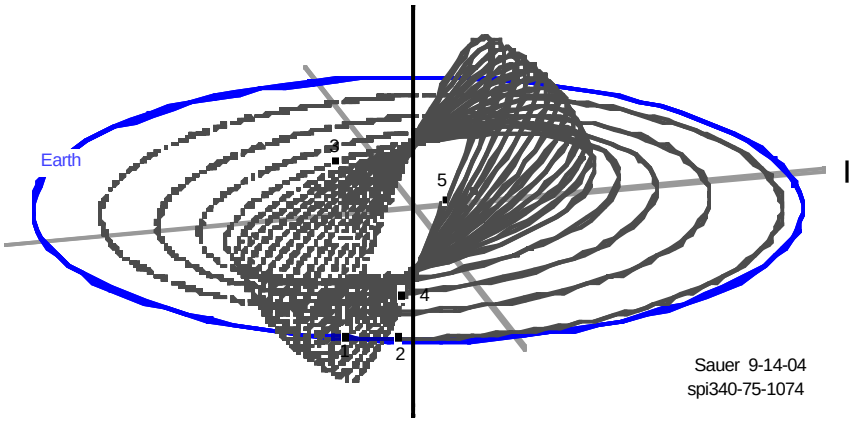

Figure 1. 3D plot of the SPI reference trajectory (credits: Carl Sauer)

then to use the large available solar radiation pressure to crank the orbit. This way, the steering strategy to reach the SPI target orbit is divided into two phases. The goal of the first phase is to spiral inwards to 0.48 AU (thereby the inclination of the SPI reference trajectory is already changed by 15 deg). The goal of the second phase is to crank the orbit until the target inclination of 75 deg is reached. This way, the SPI target orbit is attained after 6.7 years. Because the solar sail film temperature does not exceed 100°C, which is quite conservative for currently projected solar sail film materials, we have dubbed this scenario "cold" mission scenario.

We have conjectured that the SPI target orbit might be attained faster using a so-called "hot" mission scenario, where the sail spirals closer to the sun than 0.48 AU, then cranks the orbit to about 75 deg, and then spirals outwards again. This way, the steering strategy to reach the SPI target orbit can be divided into three phases. We have used InTrance (see Refs. 9 and 10), a method that combines artificial neural networks and evolutionary algorithms, to find a near-globally optimal trajectory. For our calculations, we have used the model for a non-perfectly reflecting solar sail with a sail temperature limit of 240°C and $C_3 = 0\,\mathrm{km}^2/\mathrm{s}^2$. The resulting trajectory is shown in Fig. 2. This "hot" trajectory takes only 4.7 years.

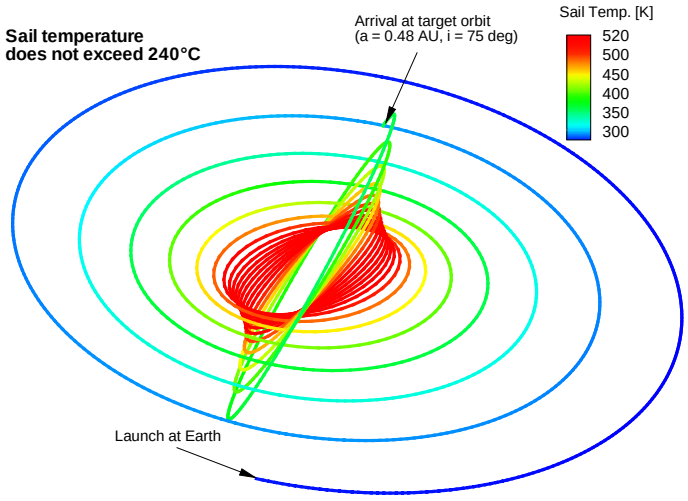

Figure 2. 3D trajectory plot for our "hot" mission scenario

The critical technologies required for the proposed mission include the deployment and control of a 160 m × 160 m solar sail and the development of a solar sail and a micro-spacecraft bus that is able to withstand the extreme space environment at less than only 0.25 AU from the sun. A 160 m × 160 m solar sail is currently not available. However, a 20 m × 20 m solar sail structure was already deployed on ground in a simulated gravity-free environment at DLR in December 1999, a 40 m × 40 m solar sail is being developed by

NASA and industries for a possible flight-validation experiment within 10 years, and thus a 160 m × 160 m solar sail is expected to be available within about 15-20 years of a sharply pursued technology development program.

Before we describe our results for the "cold" mission scenario (section V) and for the "hot" mission scenario (section VI), we will briefly outline the employed solar sail force model for non-perfect reflection (section II), our simulation model (section III), and the used trajectory optimization methods (section IV).

II. Solar Sail Force Model

For the description of the solar radiation pressure (SRP) force exerted on a solar sail, it is convenient to introduce two unit vectors. The first one is the sail normal vector $\boldsymbol{n}$, which is perpendicular to the sail surface and always directed away from the sun. Let $\mathcal{O} = \{\boldsymbol{e}_r, \boldsymbol{e}_t, \boldsymbol{e}_h\}$ be an orthogonal right-handed coordinate frame, where $\boldsymbol{e}_r$ points always along the sun-spacecraft line, $\boldsymbol{e}_h$ is the orbit plane normal (pointing along the spacecraft's orbital angular momentum vector), and $\boldsymbol{e}_t$ completes the right-handed coordinate system ($\boldsymbol{e}_r \times \boldsymbol{e}_t = \boldsymbol{e}_h$). Then in $\mathcal{O}$, the direction of the sail normal vector, which describes the sail attitude, is expressed by the pitch angle α and the clock angle δ (Fig. 3). The second unit vector is the thrust unit vector $\boldsymbol{m}$, which points along the direction of the SRP force. Its direction is described likewise by the cone angle θ and the clock angle δ.

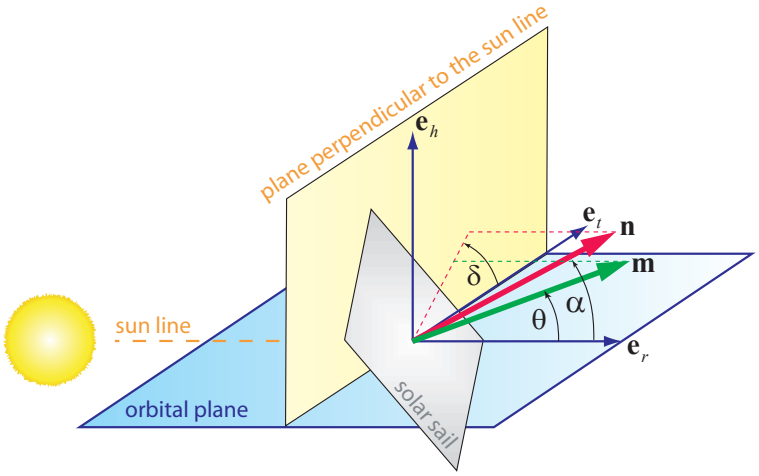

Figure 3. Definition of the sail normal vector and the trust normal vector

At a distance r from the sun, the SRP is

$$P = \frac{S_0}{c}\left(\frac{r_0}{r}\right)^2 = 4.563\,\frac{\mu\mathrm{N}}{\mathrm{m}^2}\cdot\left(\frac{r_0}{r}\right)^2 \tag{1}$$

where $S_0 = 1368\,\mathrm{W/m^2}$ is the solar constant, c is the speed of light in vacuum, and $r_0 = 1\,\mathrm{AU}$.

In this paper, the standard SRP force model for non-perfect reflection from Ref. 11 by Wright is employed, which uses the set of optical coefficients $\mathcal{P} = \{\rho, s, \varepsilon_\mathrm{f}, \varepsilon_\mathrm{b}, B_\mathrm{f}, B_\mathrm{b}\}$ to parameterize the optical characteristics of the sail film, where ρ is the reflection coefficient, s is the specular reflection factor, ε_f and ε_b are the emission coefficients of the front and back side, respectively, and B_f and B_b are the non-Lambertian coefficients of the front and back side, respectively, which describe the angular distribution of the emitted and the diffusely reflected photons. According to Ref. 11, the optical coefficients for a solar sail with a highly reflective aluminum-coated front side and a highly emissive chromium-coated back side (to keep the sail temperature moderate) are $\mathcal{P}_{\mathrm{Al|Cr}} = \{\rho = 0.88, s = 0.94, \varepsilon_\mathrm{f} = 0.05, \varepsilon_\mathrm{b} = 0.55, B_\mathrm{f} = 0.79, B_\mathrm{b} = 0.55\}$. It can be shown (see Ref. 12) that in a sail-fixed 2D coordinate frame $\mathcal{S} = \{\boldsymbol{n}, \boldsymbol{t}\}$ (see Fig. 4; because of symmetry, the third dimension is not relevant here), the SRP force exerted on the solar sail has a normal component $F_\perp$ (along $\boldsymbol{n}$) and a tangential component $F_{||}$ (along $\boldsymbol{t}$) with

$$F_\perp = \boldsymbol{F}_\mathrm{SRP}\cdot\boldsymbol{n} = 2PA\cos\alpha\,\psi_\perp \tag{2a}$$

$$F_{||} = \boldsymbol{F}_\mathrm{SRP}\cdot\boldsymbol{t} = -2PA\cos\alpha\,\psi_{||} \tag{2b}$$

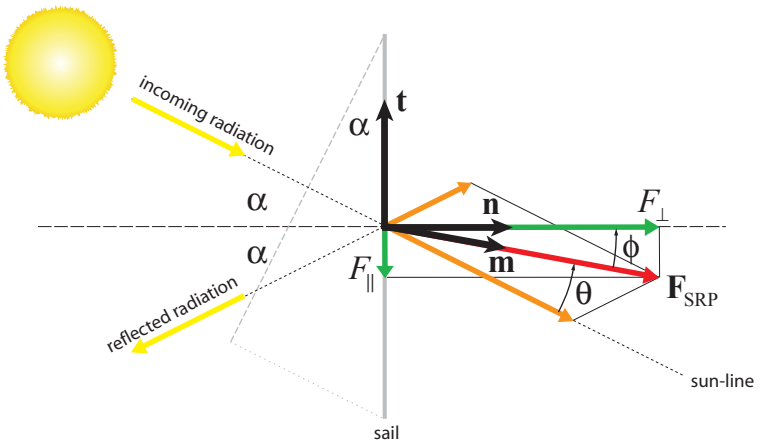

Figure 4. SRP force on a solar sail according to the non-perfectly reflecting force model

where A is the sail area and

$$\psi_\perp = a_1 \cos\alpha + a_2 \tag{3a}$$

$$\psi_{||} = a_3 \sin\alpha \tag{3b}$$

with

$$a_1 \triangleq \frac{1}{2}(1+s\rho) \qquad a_2 \triangleq \frac{1}{2}\left[B_\mathrm{f}(1-s)\rho + (1-\rho)\frac{\varepsilon_\mathrm{f}B_\mathrm{f} - \varepsilon_\mathrm{b}B_\mathrm{b}}{\varepsilon_\mathrm{f}+\varepsilon_\mathrm{b}}\right] \qquad a_3 \triangleq \frac{1}{2}(1-s\rho) \tag{4}$$

By defining $\Psi \triangleq (\psi_\perp^2 + \psi_{||}^2)^{1/2}$, the total SRP force vector may then be written as

$$\boldsymbol{F}_{\mathrm{SRP}} = 2PA\cos\alpha\,\Psi\,\boldsymbol{m} \tag{5}$$

where Ψ depends only on the pitch angle α and the optical coefficients $\mathcal{P}$ of the sail film. The angle between $\boldsymbol{m}$ and $\boldsymbol{n}$, $\phi = \arctan(\psi_{||}/\psi_\perp)$, is called the centerline angle. The cone angle, i.e. the angle between $\boldsymbol{m}$ and the radial unit vector $\boldsymbol{e}_r$, is then $\theta = \alpha - \phi = \alpha - \arctan(\psi_{||}/\psi_\perp)$.

The most commonly used solar sail performance parameter is the characteristic acceleration a_c. It is defined as the SRP acceleration acting on a solar sail that is oriented perpendicular to the sun line ($\boldsymbol{n} \equiv \boldsymbol{e}_r$) at r_0 (1 AU). For the non-perfectly reflecting SRP force model, it is

$$a_c = \frac{2P_0A}{m}(a_1 + a_2) \tag{6}$$

where $P_0 = P(r = r_0)$ and m is the sailcraft mass.

III. Simulation Model

Besides the gravitational forces of all celestial bodies and the SRP force, many disturbing forces influence the motion of solar sails in space, as they are caused, e.g., by the solar wind, the finiteness of the solar disk, the reflected light from close celestial bodies, and the aberration of solar radiation (Poynting-Robertson effect). Furthermore, a real solar sail bends and wrinkles, depending on the actual solar sail design (Ref. 13). All these issues have to be considered for high precision trajectory determination and control. For mission feasibility analysis, however, as it is done within this paper, the following simplifications can be made:

1. The solar sail is a flat plate.
2. The solar sail is moving under the sole influence of solar gravitation and radiation.
3. The sun is a point mass and a point light source.
4. The solar sail attitude can be changed instantaneously.

Let the reference frame $\mathcal{I} = \{\boldsymbol{e}_x, \boldsymbol{e}_y, \boldsymbol{e}_z\}$ be a heliocentric inertial right-handed coordinate frame. The equations of motion for a solar sail in the $\mathcal{I}$-frame are:

$$\dot{\boldsymbol{r}} = \boldsymbol{v}, \qquad \dot{\boldsymbol{v}} = -\frac{\mu}{r^3}\,\boldsymbol{r} + \frac{\boldsymbol{F}_{\text{SRP}}}{m} + \boldsymbol{a}_d \tag{7}$$

where $\boldsymbol{r} = (r_x, r_y, r_z)$ is the solar sail position, $\boldsymbol{v} = (v_x, v_y, v_z)$ is the solar sail velocity, μ is the sun's gravitational parameter, and $\boldsymbol{a}_d$ is the disturbing acceleration, which is – according to the simplifications made above – neglected within this paper.

IV. Trajectory Optimization Methods

A. Local Steering Laws

Although local steering laws (LSLs) are not a trajectory optimization method in the narrower sense, they give the locally optimal thrust direction to change some specific osculating orbital element of the spacecraft with a locally maximum rate. To obtain LSLs, Lagrange's planetary equations in Gauss' form may be used, which describe the rate of change of a body's osculating orbital elements due to some (propulsive and/or disturbing) acceleration. This can best be done in the orbit frame $\mathcal{O} = \{\boldsymbol{e}_r, \boldsymbol{e}_t, \boldsymbol{e}_h\}$. According to Ref. 14, the equations for the semi-major axis a, the eccentricity e, and the inclination i can be written as

$$\frac{da}{dt} = \frac{2a^2}{h}\left(e\sin f a_r + (p/r)\,a_t\right) \tag{8a}$$

$$\frac{de}{dt} = \frac{1}{h}\left(p\sin f a_r + \left[(p+r)\cos f + re\right]a_t\right) \tag{8b}$$

$$\frac{di}{dt} = \frac{1}{h} r\cos(\omega + f) a_h \tag{8c}$$

where a_r, a_t, and a_h are the acceleration components along the $\mathcal{O}$-frame unit vectors, $h = |\boldsymbol{h}|$ is the orbital angular momentum per spacecraft unit mass, ω is the argument of perihelion, f is the true anomaly, and p is the semilatus rectum of the orbit. Because Eqs. (8) can be written as

$$\frac{da}{dt} = \frac{2a^2}{h}\begin{pmatrix} e\sin f \\ p/r \\ 0 \end{pmatrix} \cdot \begin{pmatrix} a_r \\ a_t \\ a_h \end{pmatrix} = \boldsymbol{k}_a \cdot \boldsymbol{a} \tag{9a}$$

$$\frac{de}{dt} = \frac{1}{h}\begin{pmatrix} p\sin f \\ (p+r)\cos f + re \\ 0 \end{pmatrix} \cdot \begin{pmatrix} a_r \\ a_t \\ a_h \end{pmatrix} = \boldsymbol{k}_e \cdot \boldsymbol{a} \tag{9b}$$

$$\frac{di}{dt} = \frac{1}{h}\begin{pmatrix} 0 \\ 0 \\ r\cos(\omega + f) \end{pmatrix} \cdot \begin{pmatrix} a_r \\ a_t \\ a_h \end{pmatrix} = \boldsymbol{k}_i \cdot \boldsymbol{a} \tag{9c}$$

it is clear that to decrease (increase) the semi-major axis with a maximum rate, the thrust vector has to be along the direction $-\boldsymbol{k}_a$ ($\boldsymbol{k}_a$), which yields the local steering law $\mathcal{L}_{a^-}$ ($\mathcal{L}_{a^+}$). To decrease the eccentricity with a maximum rate, the thrust vector has to be along the direction $-\boldsymbol{k}_e$ ($\mathcal{L}_{e^-}$), and to increase the inclination with a maximum rate, the thrust vector has to be along the direction $\boldsymbol{k}_i$ ($\mathcal{L}_{i^+}$). Unlike for other spacecraft, however, where the thrust vector can be directed into any desired direction, the SRP force vector of a solar sail is constrained to lie on a "bubble" that is directed away from the sun. Therefore, when using LSLs, the projection of the SRP force vector onto the respective $\boldsymbol{k}$-vector has to be maximized.

B. Evolutionary Neurocontrol

Within this paper, evolutionary neurocontrol (ENC) is used to calculate near-globally optimal trajectories. This method is based on a combination of artificial neural networks (ANNs) with evolutionary algorithms (EAs). ENC attacks low-thrust trajectory optimization problems from the perspective of artificial intelligence and machine learning. Here, it can only be sketched how this method is used to search for optimal solar sail

trajectories. The reader who is interested in the details of the method is referred to Refs. 9, 10, and 15. The problem of searching an optimal solar sail trajectory $\boldsymbol{x}^\star[t] = (\boldsymbol{r}^\star[t], \dot{\boldsymbol{r}}^\star[t])$ – where the symbol "$[t]$" denotes the time history of the preceding variable and the symbol "$\star$" denotes its optimal value – is equivalent to the problem of searching an optimal sail normal vector history $\boldsymbol{n}^\star[t]$, as it is defined by the optimal time history of the so-called direction unit vector $\boldsymbol{d}^\star[t]$, which points along the optimal thrust direction. Within the context of machine learning, a trajectory is regarded as the result of a sail steering strategy S that maps the problem relevant variables (the solar sail state $\boldsymbol{x}$ and the target state $\boldsymbol{x}_\mathrm{T}$) onto the direction unit vector, $\mathsf{S} : \{\boldsymbol{x}, \boldsymbol{x}_\mathrm{T}\} \subset \mathbb{R}^{12} \mapsto \{\boldsymbol{d}\} \subset \mathbb{R}^3$, from which $\boldsymbol{n}$ is calculated. This way, the problem of searching $\boldsymbol{x}^\star[t]$ is equivalent to the problem of searching (or learning) the optimal sail steering strategy $\mathsf{S}^\star$. An ANN may be used as a so-called neurocontroller (NC) to implement solar sail steering strategies. It can be regarded as a parameterized function $\mathsf{N}_{\boldsymbol{\pi}}$ (the network function) that is – for a fixed network topology – completely defined by the internal parameter set $\boldsymbol{\pi}$ of the ANN. Therefore, each $\boldsymbol{\pi}$ defines a sail steering strategy $\mathsf{S}_{\boldsymbol{\pi}}$. The problem of searching $\boldsymbol{x}^\star[t]$ is therefore equivalent to the problem of searching the optimal NC parameter set $\boldsymbol{\pi}^\star$. EAs that work on a population of strings can be used for finding $\boldsymbol{\pi}^\star$ because $\boldsymbol{\pi}$ can be mapped onto a string $\boldsymbol{\xi}$ (also called chromosome or individual). The trajectory optimization problem is solved when the optimal chromosome $\boldsymbol{\xi}^\star$ is found. Figure 5 sketches the subsequent transformation of a chromosome into a solar sail trajectory. An evolutionary neurocontroller (ENC) is a NC that employs an EA for learning (or breeding) $\boldsymbol{\pi}^\star$. ENC was implemented within a low-thrust trajectory optimization program called InTrance, which stands for **In**telligent **Tra**jectory optimization using **n**euro**c**ontroller **e**volution. InTrance is a smart global trajectory optimization method that requires only the target body/state and intervals for the initial conditions (e.g., launch date, hyperbolic excess velocity, etc.) as input to find a near-globally optimal trajectory for the specified problem. It works without an initial guess and does not require the attendance of a trajectory optimization expert.

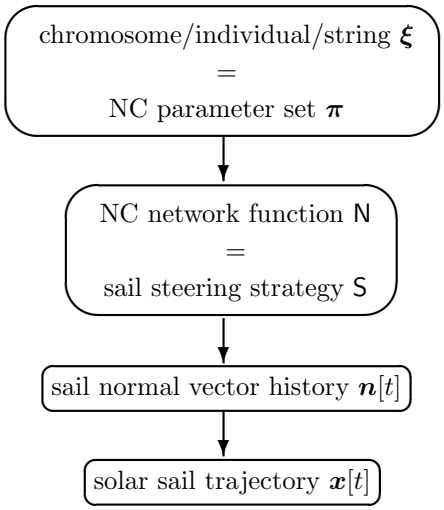

Figure 5. Transformation of a chromosome into a solar sail trajectory

V. Optimization of the "Cold" Mission Scenario

Our baseline mission design foresees a non-perfectly reflecting solar sail with a characteristic acceleration of $a_c = 0.35\,\mathrm{mm/s^2}$. Although the reference mission, as it is described in Refs. 4 and 5, uses a hyperbolic excess energy of $C_3 = 0.25\,\mathrm{km^2/s^2}$ for interplanetary insertion, our baseline mission design is based on $C_3 = 0\,\mathrm{km^2/s^2}$ to make the different calculations better comparable.

It was first found by Wright in Refs. 6 and 7 and further examined by Sauer in Ref. 8 that the best way to crank a solar sail orbit is to first spiral inwards to a close solar distance, and then to use the large available SRP to change the inclination. Using LSLs, the strategy to attain the SPI target orbit divides the trajectory into the following phases:

1: Spiralling inwards until the SPI target semi-major axis is reached using local steering law $\mathcal{L}_{a^-}$ (the

inclination stays constant during this phase)

2_A: Cranking the orbit until the SPI target inclination is reached using local steering law $\mathcal{L}_{i^+}$ (the semi-major axis stays nearly constant during this phase).

2_B: Circularizing the orbit until the SPI target orbit is attained using a combination of the local steering laws $\mathcal{L}_{a^-}$, $\mathcal{L}_{a^+}$, and $\mathcal{L}_{e^-}$ (because only the inclination but not the semi-major axis stays constant when only $\mathcal{L}_{e^-}$ is applied)

The transition between phase 2_A and 2_B is quite indistinct. Therefore, both phases can be seen as a single phase, phase 2. Additionally, using LSLs, the "optimization" of phase 2_B is quite tricky. Therefore, when later in this paper LSLs are applied, phase 2_B will be neglected, i.e. phase $2 \equiv$ phase 2_A in this case. The transfer time is then $\Delta t = \Delta t_1 + \Delta t_2$.

If solar sail degradation is not considered, the acceleration capability of a solar sail increases $\propto 1/r^2$ when going closer to the sun. The minimum solar distance, however, is constrained by the temperature limit of the sail film T_{lim} and the spacecraft (here, however, we consider only the temperature limit of the sail film but not of the spacecraft). The equilibrium temperature of the sail film is (see Ref. 12)

$$T = \left[\frac{S_0}{\sigma} \frac{1-\rho}{\varepsilon_f + \varepsilon_b} \left(\frac{r_0}{r} \right)^2 \cos\alpha \right]^{1/4} \tag{10}$$

where $\sigma = 5.67 \times 10^{-8}\,\mathrm{Wm^{-2}K^{-4}}$ is the Stefan-Boltzmann constant. Thus the sail temperature does not only depend on the solar distance, but also on the sail attitude, $T = T(r, \alpha)$ (and of course on the set of optical parameters $\mathcal{P}$). To prevent the solar sail from approaching the sun too closely, Sauer has used a minimal solar distance r_{lim} instead of a temperature limit T_{lim}, probably to keep the trajectory calculations simple. Note that a direct T_{lim}-constraint can be realized by constraining the pitch angle α (that is also the light incidence angle) in a way that it cannot become smaller than the critical pitch angle, where T_{lim} would be exceeded, i.e. $\alpha > \alpha_{\mathrm{lim}}(r, T_{\mathrm{lim}})$. Although we could not find an explicit solar sail film temperature limit for the SPI mission in the literature, our re-calculation of the reference mission has shown that the solar sail temperature does not exceed 100°C (see also Fig.7(d)). Therefore, we have chosen this temperature as the sail temperature limit for the calculations in this section, i.e. $T_{\mathrm{lim}} = 100°\mathrm{C}$. Because this temperature limit is very conservative for currently projected solar sail film materials, we have dubbed this scenario "cold" mission scenario. Later, in section VI, we will also investigate "hot" mission scenarios, as they can be applied for higher sail temperature limits ($T_{\mathrm{lim}} \geq 200°\mathrm{C}$).

Although orbit cranking is most effective for a circular orbit, it is also important to consider elliptic orbits. Therefore, we describe the optimal orbit-cranking behavior rather by an orbit-cranking semi-major axis a_{cr} instead of an orbit-cranking radius. Using the direct sail temperature constraint, a_{cr} defines the time Δt_2 that is required to crank the orbit to the required inclination. Δt_2 is influenced by two adverse effects, leading to an optimal orbit-cranking semi-major axis $a_{\mathrm{cr,opt}}(T_{\mathrm{lim}})$ where the inclination change rate $\Delta i/\Delta t$ is maximal and thus Δt_2 is minimal, as it can be seen from Fig. 6. For $a_{\mathrm{cr}} > a_{\mathrm{cr,opt}}$, the inclination

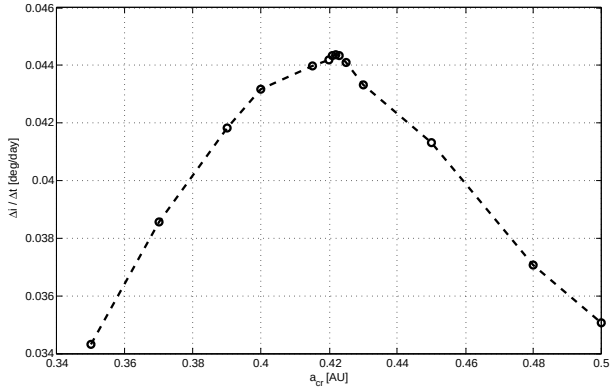

Figure 6. "Cold" mission scenario: Inclination change rate over orbit-cranking semi-major axis ($T_{\mathrm{lim}} = 100°\mathrm{C}$, $a_c = 0.35\,\mathrm{mm/s^2}$), circular orbit

change takes longer than for $a_{\mathrm{cr,opt}}$ because of the lower SRP. For $a_{\mathrm{cr}} < a_{\mathrm{cr,opt}}$, the inclination change also takes longer than for $a_{\mathrm{cr,opt}}$ because of the (inefficiently) large critical pitch angle α_{lim} that is required to keep $T < T_{\mathrm{lim}}$. Thus $\Delta t_2 = \Delta t_2(T_{\mathrm{lim}})$. It can be seen from Fig. 6 that $a_{\mathrm{cr,opt}}(T_{\mathrm{lim}} = 100°\mathrm{C}) = 0.422\,\mathrm{AU}$ where $\Delta i/\Delta t(T_{\mathrm{lim}} = 100°\mathrm{C}, a_c = 0.35\,\mathrm{mm/s^2}) = 0.0444\,\mathrm{deg/day}$.

We have used three different methods to calculate solar sail trajectories for the "cold" mission scenario:

1. **LSLs:** The local steering laws $\mathcal{L}_{a^-}$ and $\mathcal{L}_{i^+}$ were applied as described above.
2. **InTrance + LSL:** InTrance was used to calculate a near-globally optimal transfer to a circular 0.48 AU-orbit with an inclination of 15 deg (as for the reference mission described in Refs. 4 and 5), and then the local steering law $\mathcal{L}_{i^+}$ was applied.
3. **InTrance:** InTrance was used to calculate a near-globally optimal transfer to the SPI target orbit.

Table 1 shows the obtained results and Fig. 7 shows the variation of the inclination, the semi-major axis, and the sail film temperature along the trajectory.

Table 1. "Cold" mission scenario results

Method	Transfer duration		$T_{\max}$	Δa	Δe	Δi
	[days]	[years]	[°C]	$[10^{-4}\mathrm{AU}]$	$[10^{-2}]$	[deg]
LSLs	2658	7.28	95	0.2	5.8	0.0
InTrance + LSL	2513	6.88	91	2.6	7.2	0.0
InTrance	2334	6.39	100	3.1	0.9	0.1

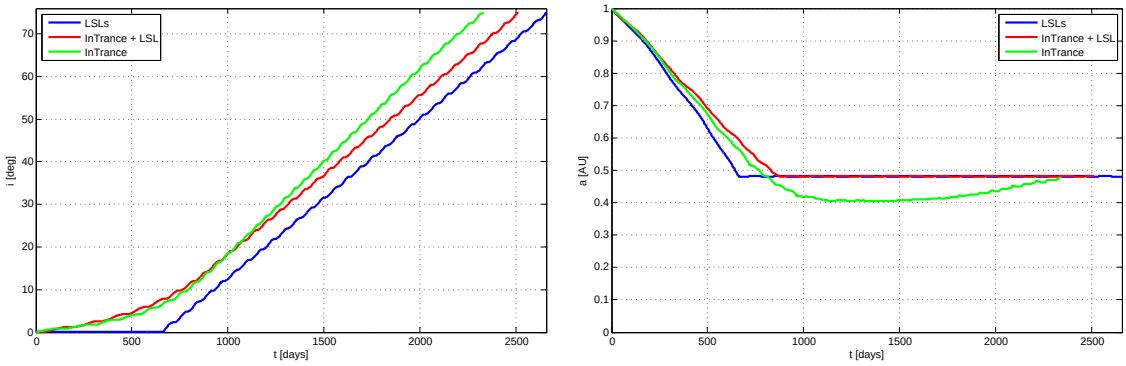

(a) Inclination over flight time, $i(t)$

(b) Semi-major axis over flight time, $a(t)$

(c) Inclination over semi-major axis, $i(a)$

(d) Sail film temperature over flight time, $T(t)$

Figure 7. "Cold" mission scenario: Comparison of different solutions

Looking at Table 1 and Fig. 7, one can clearly see that using local steering laws and patching together the solutions of phase 1 and 2 yields a suboptimal solution. The (InTrance+LSL)-trajectory is 145 days

faster than the LSL-trajectory. It proves that the optimal trajectory has a smooth transition between the two phases, changing the inclination also during phase 1, whenever the sailcraft is close to the nodes. The InTrance-solution approaches the sun much closer than 0.48 AU, as can be seen from Figs. 7(b) and 7(c). The closest solar distance is only 0.407 AU (we note that this is smaller than $a_{\mathrm{cr,opt}}$). This closer solar distance yields a higher inclination change rate so that the target inclination is reached earlier (without exceeding the sail temperature limit of 100°C). This result shows that faster trajectories can be obtained for a given sail temperature limit T_{lim}, if not a minimum solar distance r_{lim} but T_{lim} is used directly as a constraint.

VI. Optimization of a Faster "Hot" Mission Scenario

Because a sail temperature limit of 100°C is quite conservative for currently projected solar sail films, we now release this constraint and use a sail temperature limit of 240°C. This way, the sail can approach the sun closer. It can be seen from Fig. 8 that $a_{\mathrm{cr,opt}}(T_{\mathrm{lim}} = 240°\mathrm{C}) = 0.22\,\mathrm{AU}$ where $\Delta i/\Delta t(T_{\mathrm{lim}} = 240°\mathrm{C}, a_c = 0.35\,\mathrm{mm/s^2}) = 0.1145\,\mathrm{deg/day}$ and thus much higher than for $T_{\mathrm{lim}} = 100°\mathrm{C}$.

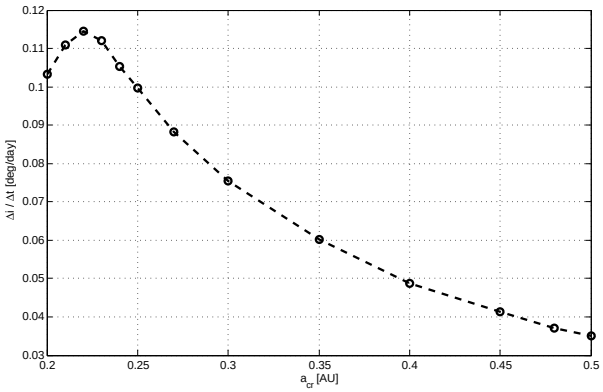

Figure 8. "Hot" mission scenario: Inclination change rate over orbit-cranking semi-major axis ($T_{\mathrm{lim}} = 240°\mathrm{C}$, $a_c = 0.35\,\mathrm{mm/s^2}$), circular orbit

Using local steering laws, the "hot" scenario to attain the SPI target orbit divides the trajectory into the following phases:

A: Spiralling inwards until the optimum solar distance for cranking the orbit is reached using local steering law $\mathcal{L}_{a^-}$ (the inclination stays constant during this phase)

B: Cranking the orbit until the SPI target inclination is reached using local steering law $\mathcal{L}_{i^+}$ (the semi-major axis stays nearly constant during this phase).

C_1: Spiralling outwards until the SPI target semi-major is reached using local steering law $\mathcal{L}_{a^+}$ (the inclination stays constant during this phase)

C_2: Circularizing the orbit until the SPI target orbit is attained using a combination of the local steering laws $\mathcal{L}_{a^-}$, $\mathcal{L}_{a^+}$ and $\mathcal{L}_{e^-}$ (because only the inclination but not the semi-major axis stays constant when only $\mathcal{L}_{e^-}$ is applied)

The transition between phase C_1 and C_2 is quite indistinct. Therefore, both phases can be seen as a single phase, phase C. Additionally, using LSLs, the "optimization" of phase C_2 is quite tricky. Therefore, phase C_2 will be neglected when LSLs are applied, i.e. phase C $\equiv$ phase C_1 in this case. The transfer time is then $\Delta t = \Delta t_{\mathrm{A}} + \Delta t_{\mathrm{B}} + \Delta t_{\mathrm{C}}$.

We have used two different methods to calculate solar sail trajectories for the "hot" mission scenario:

1. **LSLs:** The local steering laws $\mathcal{L}_{a^-}$, $\mathcal{L}_{i^+}$, and $\mathcal{L}_{a^+}$ were applied as described above.

2. **InTrance:** InTrance was used to calculate a near-globally optimal transfer to the SPI target orbit.

Table 2 shows the obtained results and Fig. 9 shows the variation of the inclination, the semi-major axis, and the sail film temperature along the trajectory. Figure 10 shows the trajectory, the variation of selected orbital elements, and the control angles for the LSL-solution, while Fig. 11 shows the same for the InTrance-solution. Looking at the relatively large final eccentricity in Fig. 10(c), one can see that phase C_2 has been omitted. Due to the poor *local* search behavior of InTrance (note that the control angles are determined by a neural network!), some "noise" remains in the control angles (Fig. 11(d)). Further fine-tuning of the solution with a local trajectory optimization method might therefore yield a marginally shorter (but probably also less robust) trajectory.

Table 2. "Hot" mission scenario results

Method	Transfer duration		$T_{\max}$	Δa	Δe	Δi
	[days]	[years]	[°C]	$[10^{-4}\text{AU}]$	$[10^{-2}]$	[deg]
LSLs	1771.5	4.85	240	0.1	8.5	0.1
InTrance	1703.0	4.66	240	1.2	0.4	0.1

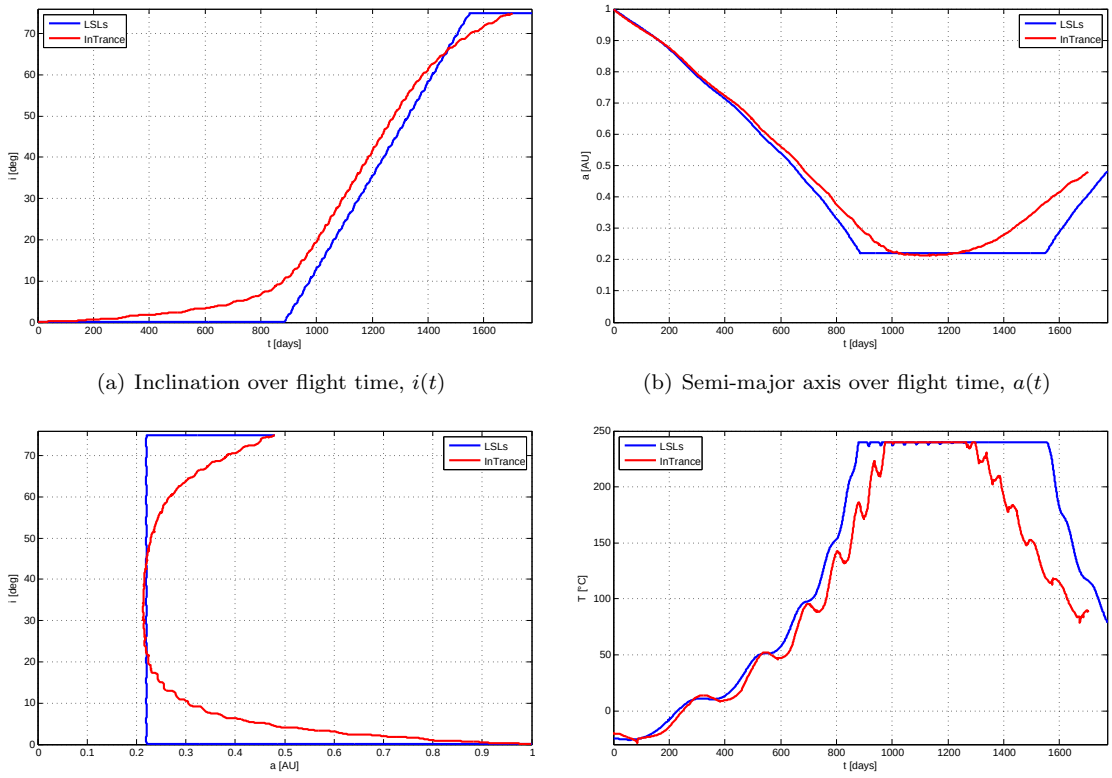

(a) Inclination over flight time, $i(t)$

(b) Semi-major axis over flight time, $a(t)$

(c) Inclination over semi-major axis, $i(a)$

(d) Sail film temperature over flight time, $T(t)$

Figure 9. "Hot" mission scenario: Comparison of the LSL-solution with the InTrance-solution

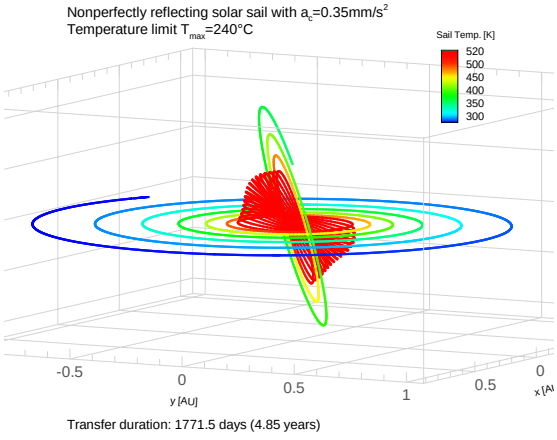

(a) 3D trajectory plot

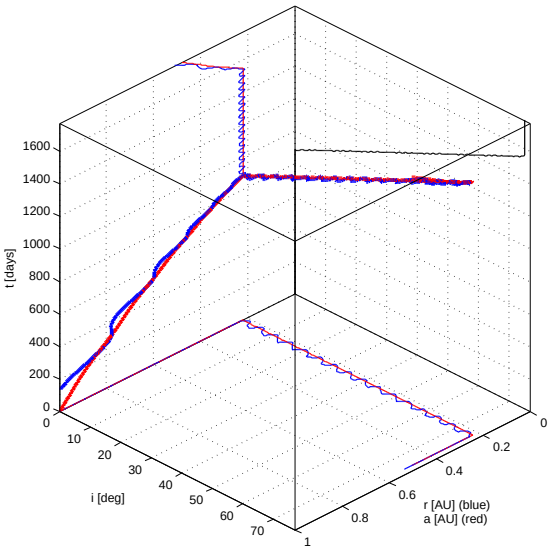

(b) i-(a,r)-t-diagram

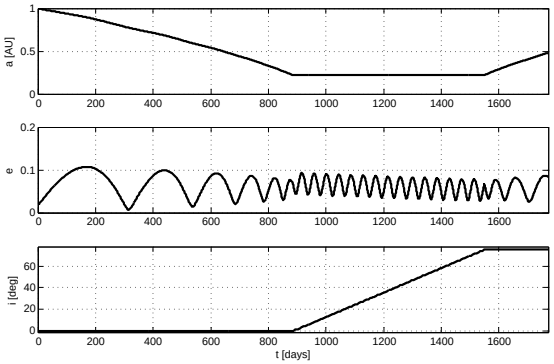

(c) Selected orbital elements

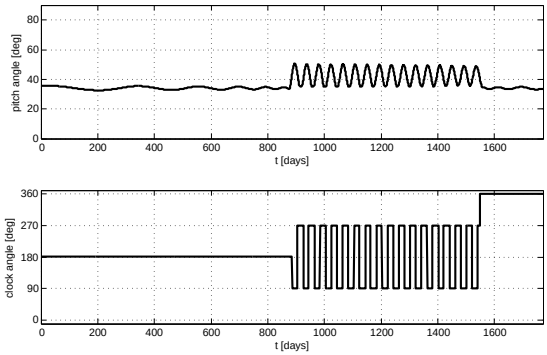

(d) Solar sail control angles

Figure 10. "Hot" mission scenario: LSL-solution

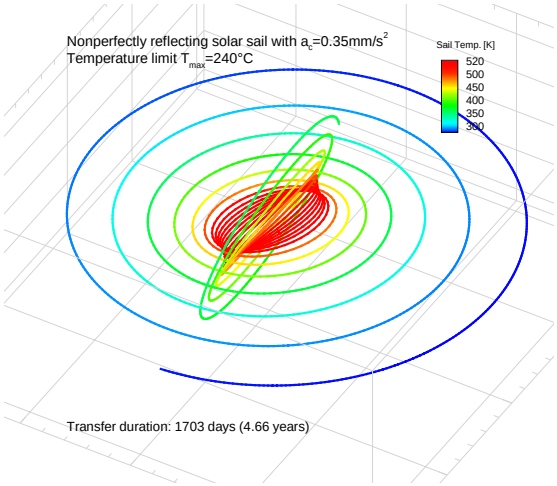

(a) 3D trajectory plot

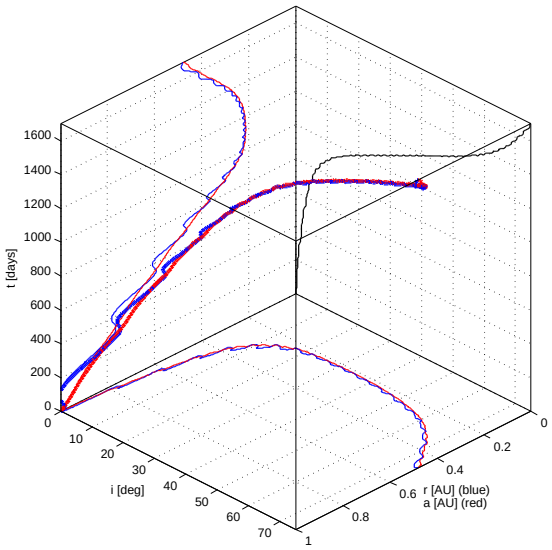

(b) i-(a,r)-t-diagram

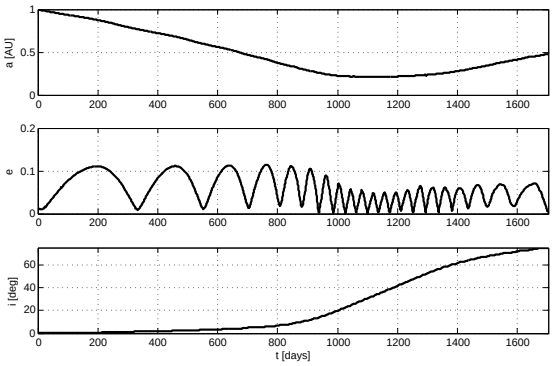

(c) Selected orbital elements

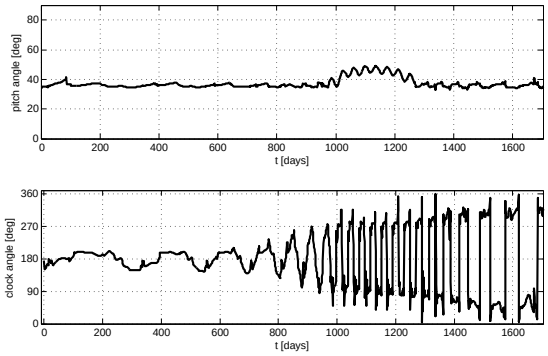

(d) Solar sail control angles

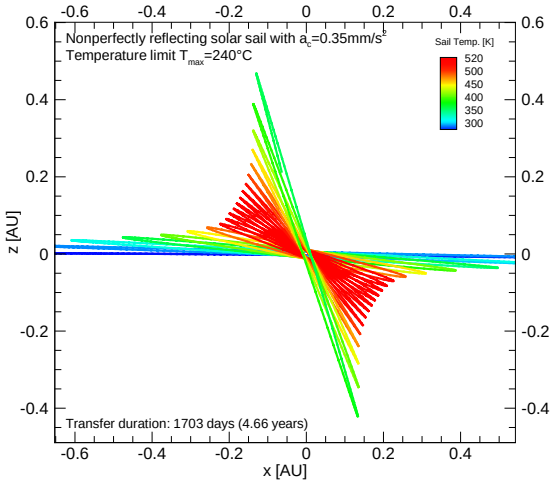

(e) x-z-trajectory plot

Figure 11. "Hot" mission scenario: InTrance-solution

A. Variation of Mission Design Parameters

1. *Variation of the Sail Temperature Limit*

In this section, the influence of the sail temperature limit T_{lim} on the SPI mission performance is investigated. Figure 12 shows for a circular orbit, how the inclination change rate varies with the orbit-cranking semi-major axis for different sail temperature limits, i.e. $(\Delta i/\Delta t)(T_{\mathrm{lim}}, a_{\mathrm{cr}})$. For $200°\mathrm{C} \leq T_{\mathrm{lim}} \leq 260°\mathrm{C}$, the optimal orbit-cranking semi-major axis can be approximated with an error of less than 2% by

$$\tilde{a}_{\mathrm{cr,opt}} \approx 1.4805 - 0.23 \cdot \ln(\tilde{T}_{\mathrm{lim}}) \tag{11}$$

where $\tilde{a}_{\mathrm{cr,opt}} = \frac{a_{\mathrm{cr,opt}}}{1\,\mathrm{AU}}$ and $\tilde{T}_{\mathrm{lim}} = \frac{T_{\mathrm{lim}}}{1°\mathrm{C}}$. The maximum inclination change rate can be approximated with an error of less than 2% by

$$\widetilde{(\Delta i/\Delta t)}_{\max} \approx 0.0113 \cdot \tilde{a}_{\mathrm{cr,opt}}^{-1.53} \tag{12}$$

where $\widetilde{(\Delta i/\Delta t)}_{\max} = \frac{(\Delta i/\Delta t)_{\max}}{1\,\mathrm{deg/day}}$.

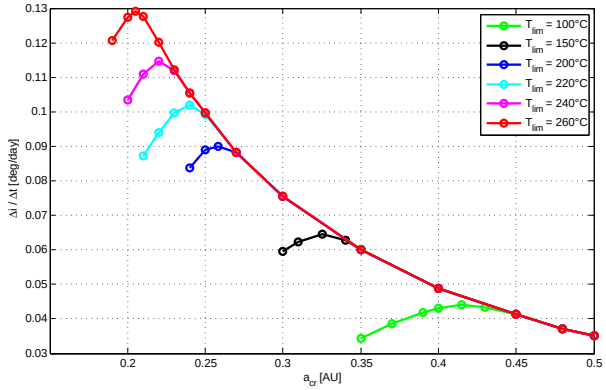

Figure 12. Inclination change rate over orbit-cranking semi-major axis for different sail temperature limits ($a_c = 0.35\,\mathrm{mm/s^2}$), circular orbit

We have used InTrance to optimize the SPI trajectory for different solar sail temperature limits ($200°\mathrm{C} \leq T_{\mathrm{lim}} \leq 260°\mathrm{C}$). The results are shown in Table 3 and Fig. 13. Figure 13(b) shows that InTrance matches the optimal orbit-cranking semi-major axes shown in Fig. 12 very closely. The transfer duration can be approximated with an error of less than 1% by

$$\Delta t(a_{\mathrm{cr,opt}}) = \Delta t_{\mathrm{A}}(a_{\mathrm{cr,opt}}) + \frac{75\,\mathrm{deg}}{(\Delta i/\Delta t)_{\max}(a_{\mathrm{cr,opt}})} + \Delta t_{\mathrm{C}}(a_{\mathrm{cr,opt}}) - \zeta \tag{13}$$

or

$$\begin{aligned}\widetilde{\Delta t}(\tilde{a}_{\mathrm{cr,opt}}) &= \Big(235 + 826\,(1 - \tilde{a}_{\mathrm{cr,opt}})\Big) + \frac{75}{0.0113 \cdot \tilde{a}_{\mathrm{cr,opt}}^{-1.53}} + \Big(30 + 771\,(0.48 - a_{\mathrm{cr,opt}})\Big) - 87 \\ &= 1374 - 1597\,\tilde{a}_{\mathrm{cr,opt}} + \frac{75}{0.0113 \cdot \tilde{a}_{\mathrm{cr,opt}}^{-1.53}}\end{aligned}$$

Table 3. Variation of T_{lim} ($a_c = 0.35\,\mathrm{mm/s^2}$, $C_3 = 0\,\mathrm{km^2/s^2}$)

T_{lim}	$a_{\mathrm{cr,opt}}$	$(\Delta i/\Delta t)_{\max}$	Transfer duration	
[°C]	[AU]	[deg/day]	[days]	[years]
200	0.260	0.0899	1793	4.90
220	0.236	0.1015	1736	4.75
240	0.220	0.1145	1679	4.60
260	0.205	0.1291	1644	4.50

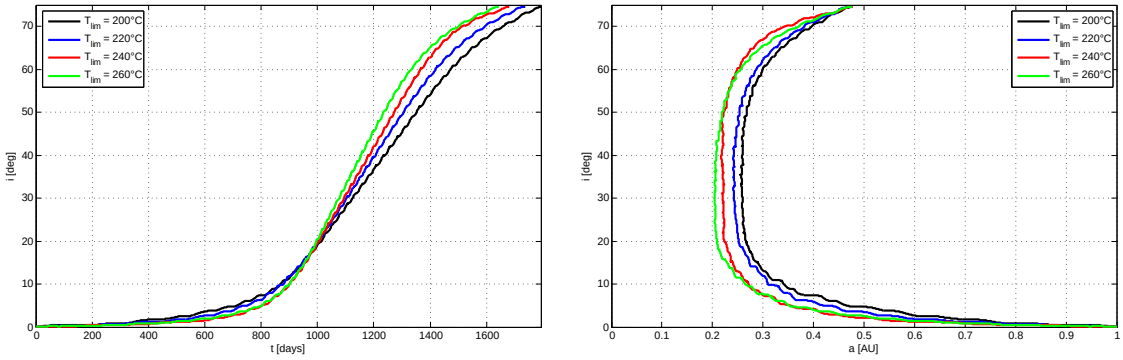

(a) Inclination over flight time, $i(t)$ (b) Inclination over semi-major axis, $i(a)$

Figure 13. Variation of $T_{\lim}$ ($a_c = 0.35\,\mathrm{mm/s^2}$, $C_3 = 0\,\mathrm{km^2/s^2}$)

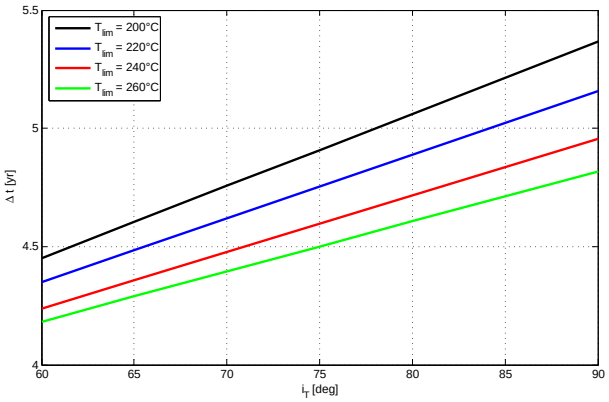

Figure 14. Approximate transfer times for different target inclinations ($a_c = 0.35\,\mathrm{mm/s^2}$, $C_3 = 0\,\mathrm{km^2/s^2}$)

where $\widetilde{\Delta t} = \frac{\Delta t}{1\,\mathrm{day}}$ and $\zeta = 87\,\mathrm{days}$ is approximately the time that can be saved by the near-globally optimal steering strategy with respect to a LSL-based steering strategy. Figure 14 shows the approximate transfer times for different target inclinations i_T and temperature limits, as they can be obtained by using

$$\Delta t(T_\mathrm{lim}, i_\mathrm{T}) = \Delta t(T_\mathrm{lim}, 75\,\mathrm{deg}) + \frac{i_\mathrm{T} - 75\,\mathrm{deg}}{(\Delta i/\Delta t)_\mathrm{max}} \tag{14}$$

Note that the transfer time for 240°C is shorter than in Table 2 because of different accuracy requirements for the fulfilment of the final constraint. In Table 2, $\Delta a \leq 10\,000\,\mathrm{km}$, $\Delta e \leq 0.01$, and $\Delta i \leq 0.3\,\mathrm{deg}$ was required, while here only $\Delta a \leq 50\,000\,\mathrm{km}$, $\Delta e \leq 0.01$, and $\Delta i \leq 0.5\,\mathrm{deg}$ was required to speed up the trajectory optimization process.

2. Variation of the Characteristic Acceleration

Next, we have investigated the influence of the characteristic acceleration a_c on the mission performance. We have used InTrance to optimize the SPI trajectory for different characteristic accelerations ($0.25\,\mathrm{mm/s^2} \leq a_c \leq 0.4\,\mathrm{mm/s^2}$). The results are shown in Table 4 and Fig. 15. Figure 15(b) shows that the optimal orbit cranking semi-major axis is independent of a_c. The transfer duration can be approximated with an error of less than 1% by

$$\widetilde{\Delta t} \approx 593/a_c \tag{15}$$

Table 4. Variation of a_c ($T_{\lim} = 240°\mathrm{C}$, $C_3 = 0\,\mathrm{km}^2/\mathrm{s}^2$)

a_c	Δt	
$[\mathrm{mm/s}^2]$	[days]	[years]
0.25	2365	6.48
0.3	1967	5.39
0.35	1679	4.60
0.4	1497	4.10

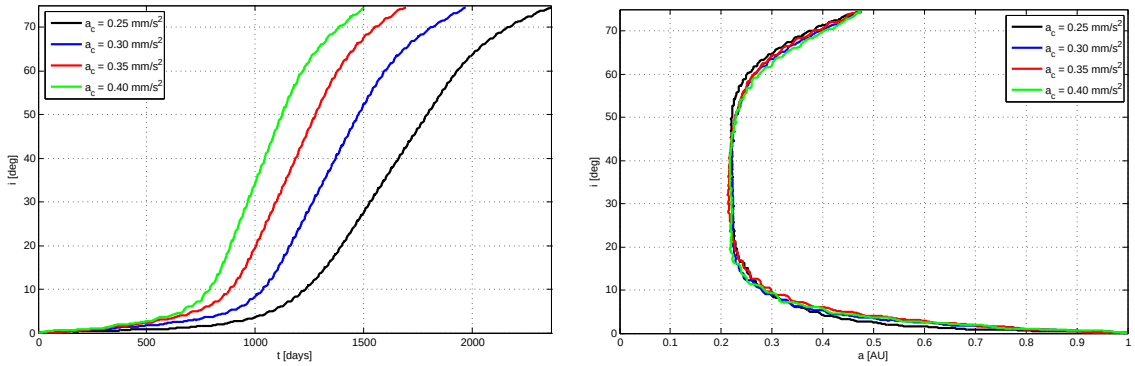

(a) Inclination over flight time, $i(t)$ (b) Inclination over semi-major axis, $i(a)$

Figure 15. Variation of a_c ($T_{\lim} = 240°\mathrm{C}$, $C_3 = 0\,\mathrm{km}^2/\mathrm{s}^2$)

3. Variation of the Hyperbolic Excess Energy for Interplanetary Insertion

Next, we have investigated the influence of the hyperbolic excess energy C_3 (or hyperbolic excess velocity $v_3 = \sqrt{C_3}$) on the mission performance. We have used InTrance to optimize the spiralling-in to a 0.48 AU circular orbit for different hyperbolic excess energies ($0\,\mathrm{km}^2/\mathrm{s}^2 \leq C_3 \leq 4\,\mathrm{km}^2/\mathrm{s}^2$). The transfer time Δt_s that can be saved by injecting the sailcraft with some hyperbolic excess velocity is shown in Fig. 16.

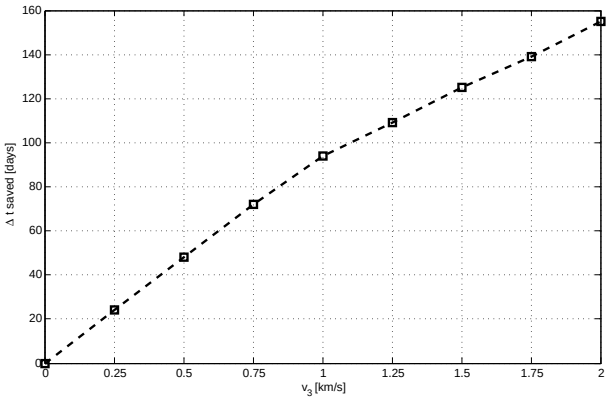

Figure 16. Variation of C_3 ($T_{\lim} = 240°\mathrm{C}$, $a_c = 0.35\,\mathrm{mm/s}^2$)

Thus a C_3 of $0.25\,\mathrm{km}^2/\mathrm{s}^2$ makes the reference trajectory from Refs. 4 and 5 about 50 days (0.13 years) faster w.r.t. to the C_3 of $0\,\mathrm{km}^2/\mathrm{s}^2$ that is used in our mission design.

B. Solar Sail Degradation

To investigate the effects of optical degradation of the sail film, as it is expected in the extreme space environment close to the sun, we apply here the parametric model developed in Ref. 16. In this parametric model the optical parameters p are assumed to depend on the cumulated solar radiation dose (SRD) $\Sigma(t)$ on the sail:

$$\frac{p(t)}{p_0} = \begin{cases} \left(1 + d\mathrm{e}^{-\lambda\Sigma(t)}\right) / (1+d) & \text{for} \quad p \in \{\rho, s\} \\ 1 + d\left(1 - \mathrm{e}^{-\lambda\Sigma(t)}\right) & \text{for} \quad p = \varepsilon_\mathrm{f} \\ 1 & \text{for} \quad p \in \{\varepsilon_\mathrm{b}, B_\mathrm{f}, B_\mathrm{b}\} \end{cases} \tag{16}$$

The (dimensionless) SRD is

$$\Sigma(t) = \frac{\tilde{\Sigma}(t)}{\tilde{\Sigma}_0} = \left(r_0^2 \int_{t_0}^{t} \frac{\cos\alpha}{r^2}\, dt' \right) \Big/ 1\,\mathrm{yr} \tag{17}$$

with $\tilde{\Sigma}_0 \triangleq S_0 \cdot 1\,\mathrm{yr} = 1368\,\mathrm{W/m^2} \cdot 1\,\mathrm{yr} = 15.768\,\mathrm{TJ/m^2}$ being the annual SRD on a surface perpendicular to the sun at 1 AU. The degradation constant λ is related to the "half life solar radiation dose" $\hat{\Sigma}$ ($\Sigma = \hat{\Sigma} \Rightarrow p = \frac{p_0 + p_\infty}{2}$) via

$$\lambda = \frac{\ln 2}{\hat{\Sigma}} \tag{18}$$

The degradation factor d defines the end-of-life values p_∞ of the optical parameters:

$$\rho_\infty = \frac{\rho_0}{1+d} \qquad s_\infty = \frac{s_0}{1+d} \qquad \varepsilon_{\mathrm{f}\infty} = (1+d)\varepsilon_{\mathrm{f}0}$$
$$\varepsilon_{\mathrm{b}\infty} = \varepsilon_{\mathrm{b}0} \qquad B_{\mathrm{f}\infty} = B_{\mathrm{f}0} \qquad B_{\mathrm{b}\infty} = B_{\mathrm{b}0}$$

Figure 17 and Table 5 show the results for different degradation factors $0 \le d \le 0.2$, assuming a half life SRD of $25\,S_0 \cdot 1\,\mathrm{yr} = 394\,\mathrm{TJ/m^2}$.

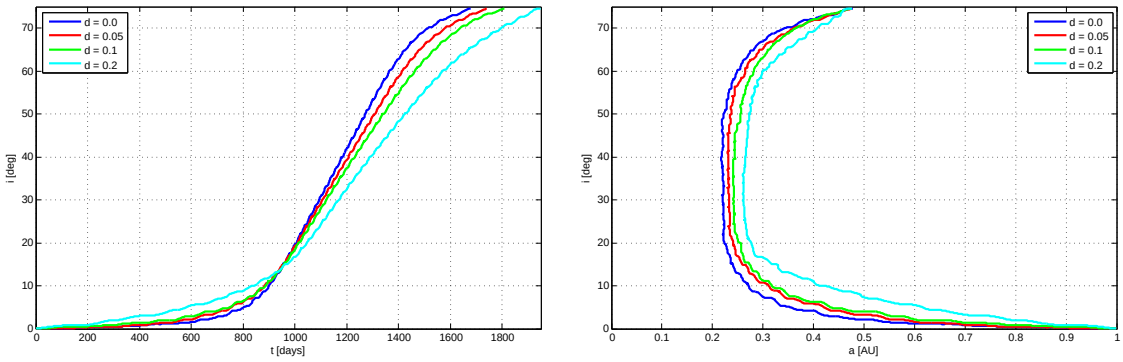

(a) Inclination over flight time, $i(t)$ (b) Inclination over semi-major axis, $i(a)$

Figure 17. Different optical degradation factors ($T_\mathrm{lim} = 240°\mathrm{C}$, $a_c = 0.35\,\mathrm{mm/s^2}$, $C_3 = 0\,\mathrm{km^2/s^2}$)

Table 5. Transfer times for different degradation factors ($T_\mathrm{lim} = 240°\mathrm{C}$, $a_c = 0.35\,\mathrm{mm/s^2}$, $C_3 = 0\,\mathrm{km^2/s^2}$)

Degradation factor	Δt [days]	[years]
0.0	1679	4.60
0.05	1742	4.77
0.1	1810	4.96
0.2	1945	5.33

For $0 \leq d \leq 0.2$, the transfer time can be approximated with an error of less than 0.2% by

$$\widetilde{\Delta t} \approx 1677 + 1335 \cdot d \tag{19}$$

The main degradation effect can be seen from Fig. 17(a), which shows that $\Delta i/\Delta t$ becomes smaller with increasing SRD. Figure 17(b) shows that for larger degradation factors it is favorable to crank the orbit further away from the sun than it would be optimal without degradation. Because optical degradation is an important factor for this mission, and because the real degradation behavior of solar sails in the space environment is to a considerable degree unknown, extensive ground and in-space tests are required prior to this mission.

VII. Conclusions

A current SPI reference mission design for the Solar Polar Imager (SPI) mission is based on a 160 m $\times$ 160 m, 450 kg square solar sail spacecraft, having a characteristic acceleration of 0.35 mm/s^2. To attain the SPI target orbit (circular orbit at 0.48 AU solar distance with 75 deg inclination), the current reference trajectory spirals inwards to 0.48 AU and then cranks the orbit to 75 deg. Because for this scenario the solar sail film temperature stays colder than 100°C, which is a conservative value, we call this a "cold" mission scenario. Using this temperature limit as a direct constraint for trajectory optimization instead of a solar distance limit, we have found a faster transfer trajectory than the reference trajectory that approaches the sun closer (to about 0.4 AU solar distance) an thus better exploits the solar radiation pressure, which is larger closer to the sun.

For higher sail temperature limits of 200-260°C, i.e. "hot" mission scenarios, we have found that the optimal transfer trajectories approach the sun even closer (to about 0.20-0.26 AU solar distance, depending on the sail temperature limit), resulting in even shorter transfer durations. Based on this "hot" mission scenario, we have also performed tradeoffs for the sail temperature limit, the characteristic acceleration and the interplanetary insertion energy to gain a deeper insight into the trade space of the SPI mission and to help the designer of such a mission to estimate the required transfer time.

By investigating different solar sail degradation behaviors, we have also found that the mission performance might be considerably affected by optical degradation of the sail surface, as it is expected in the extreme space environment close to the sun. Because the real degradation behavior of solar sails is to a considerable degree unknown, ground and in-space tests should be done prior to this mission.

Acknowledgements

The work described in this paper was funded in part by the In-Space Propulsion Technology Program, which is managed by NASA's Science Mission Directorate in Washington, D.C., and implemented by the In-Space Propulsion Technology Office at Marshall Space Flight Center in Huntsville, Alabama. The program objective is to develop in-space propulsion technologies that can enable or benefit near and mid-term NASA space science missions by significantly reducing cost, mass or travel times.

References

[1]Macdonald, M., Hughes, G., McInnes, C., Lyngvi, A., Falkner, P., and Atzei, A., "Solar Polar Orbiter: A Solar Sail Technology Reference Study," *Journal of Spacecraft and Rockets*, accepted.

[2]NASA's Sun-Earth Connection Division Website, http://sec.gsfc.nasa.gov.

[3]"Sun-Solar System Connection. Science and Technology Roadmap 2005 - 2035," NASA publication, NASA, 2005.

[4]Wie, B., Thomas, S., Paluszek, M., and Murphy, D., "Propellantless AOCS Design for a 160-m, 450-kg Sailcraft of the Solar Polar Imager Mission," 41st AIAA/ASME/SAE/ASEE Joint Propulsion Conference and Exhibit, Tucson, USA, July 2005, AIAA Paper 2005-3928.

[5]Wie, B., "Thrust Vector Control of Solar Sail Spacecraft," AIAA Guidance, Navigation, and Control Conference, San Francisco, USA, August 2005, AIAA Paper 2005-6086.

[6]Wright, J., "Solar Sailing – Evaluation of Concept and Potential," Tech. rep., Battelle Columbus Laboratories, Columbus, Ohio, March 1976, BMI-NLVP-TM-74-3.

[7]Wright, J. and Warmke, J., "Solar Sail Mission Applications," AIAA/AAS Astrodynamics Conference, San Diego, USA, August 18-20, 1976, AIAA Paper 76-808.

[8]Sauer, C., "A Comparison of Solar Sail and Ion Drive Trajectories for a Halley's Comet Rendezvous Mission," AAS/AIAA Astrodynamics Conference, Jackson, USA, September 1977, AAS Paper 77-104.

[9]Dachwald, B., *Low-Thrust Trajectory Optimization and Interplanetary Mission Analysis Using Evolutionary Neurocontrol*, Doctoral thesis, Universität der Bundeswehr München; Fakultät für Luft- und Raumfahrttechnik, 2004.

[10]Dachwald, B., "Optimization of Interplanetary Solar Sailcraft Trajectories Using Evolutionary Neurocontrol," *Journal of Guidance, Control, and Dynamics*, Vol. 27, No. 1, pp. 66–72.

[11]Wright, J., *Space Sailing*, Gordon and Breach Science Publishers, Philadelphia, 1992.

[12]McInnes, C., *Solar Sailing. Technology, Dynamics and Mission Applications*, Springer–Praxis Series in Space Science and Technology, Springer–Praxis, Berlin, Heidelberg, New York, Chicester, 1999.

[13]Garbe, G., Wie, B., Murphy, D., Ewing, A., Lichodziejewski, L., Derbes, B., Campbell, B., Wang, J., Taleghani, B., Canfield, S., Beard, J., and Peddieson, J., "Solar Sail Propulsion Technology Development," *Recent Advances in Gossamer Spacecraft*, edited by C. Jenkins, Vol. 212 of *Progress in Astronautics and Aeronautics*, American Institute of Aeronautics and Astronautics, Reston, 2006, pp. 191–261.

[14]Battin, R., *An Introduction to the Mathematics and Methods of Astrodynamics*, AIAA Education Series, American Institute of Aeronautics and Astronautics, Reston, revised ed., 1999.

[15]Dachwald, B., "Optimization of Very-Low-Thrust Trajectories Using Evolutionary Neurocontrol," *Acta Astronautica*, Vol. 57, No. 2-8, 2005, pp. 175–185.

[16]Dachwald, B., Mengali, G., Quarta, A., and Macdonald, M., "Parametric Model and Optimal Control of Solar Sails with Optical Degradation," *Journal of Guidance, Control, and Dynamics*, accepted.